Fermi National Accelerator Laboratory

FERMILAB Pub-95/032-E
E687

# Analysis of the $D^+$, $D_s^+ \to K^+K^-\pi^+$ Dalitz Plots

P.L. Frabetti et al.
The E687 Collaboration

*Fermi National Accelerator Laboratory*
*P.O. Box 500, Batavia, Illinois 60510*

March 1995

Submitted to *Physics Letters B*

Operated by Universities Research Association Inc. under Contract No. DE-AC02-76CHO3000 with the United States Department of Energy

## Disclaimer

# Analysis of the $D^+, D_s^+ \to K^+K^-\pi^+$ Dalitz Plots

## E687 Collaboration


P. L. Frabetti

Dip. di Fisica dell'Università and INFN - Bologna, I-40126 Bologna, Italy

H. W. K. Cheung [a], J. P. Cumalat, C. Dallapiccola [b], J. F. Ginkel, S. V. Greene, W. E. Johns, M. S. Nehring

University of Colorado, Boulder, CO 80309, USA

J. N. Butler, S. Cihangir, I. Gaines, P. H. Garbincius, L. Garren, S. A. Gourlay, D. J. Harding, P. Kasper, A. Kreymer, P. Lebrun, S. Shukla, M. Vittone

Fermilab, Batavia, IL 60510, USA

S. Bianco, F. L. Fabbri, S. Sarwar, A. Zallo

Laboratori Nazionali di Frascati dell'INFN, I-00044 Frascati, Italy

R. Culbertson [h], R. W. Gardner, R. Greene, J. Wiss

University of Illinois at Urbana-Champaign, Urbana, IL 61801, USA

G. Alimonti, G. Bellini, M. Boschini, D. Brambilla, B. Caccianiga, L. Cinquini [c], M. Di Corato, M. Giammarchi, P. Inzani, F. Leveraro, S. Malvezzi, D. Menasce, E. Meroni, L. Moroni, D. Pedrini, L. Perasso, F. Prelz, A. Sala, S. Sala, D. Torretta [a]

Dip. di Fisica dell'Università and INFN - Milano, I-20133 Milan, Italy

D. Buchholz, D. Claes [d], B. Gobbi, B. O'Reilly,

Northwestern University, Evanston, IL 60208, USA

J. M. Bishop, N. M. Cason, C. J. Kennedy [e], G. N. Kim [f], T. F. Lin, D. L. Puseljic [g], R. C. Ruchti, W. D. Shephard, J. A. Swiatek, Z. Y. Wu

University of Notre Dame, Notre Dame, IN 46556, USA

V. Arena, G. Boca, C. Castoldi, G. Gianini, S. P. Ratti, C. Riccardi, L. Viola, P. Vitulo

Dip. di Fisica Nucleare e Teorica dell'Università and INFN - Pavia, I-27100 Pavia, Italy

A. Lopez, University of Puerto Rico at Mayaguez, Puerto Rico

G. P. Grim, V. S. Paolone, P. M. Yager, University of California-Davis, Davis, CA 95616, USA

J. R. Wilson, University of South Carolina, Columbia, SC 29208, USA

P. D. Sheldon, Vanderbilt University, Nashville, TN 37235, USA

F. Davenport, University of North Carolina-Asheville, Asheville, NC 28804, USA

G.R. Blackett, M. Pisharody, T. Handler

University of Tennessee, Knoxville, TN 37996, USA

B. G. Cheon, J. S. Kang, K. Y. Kim

Korea University, Seoul 136-701, Korea

## Abstract

Amplitude analyses of the $D^+$ and $D_s^+ \to K^+K^-\pi^+$ Dalitz plots are presented using data collected by the Fermilab high energy photoproduction experiment E687. Our data are fit to a model consisting of a sum of Breit-Wigner amplitudes for the intermediate two-body resonant decay modes. We extract decay fractions and relative phases. These results are used to infer new branching ratios for $D^+ \to K^+K^-\pi^+$ inclusive as well as the $\phi\pi^+$ and $\overline{K}^*(892)^0K^+$ channels.

## I. INTRODUCTION

Recently, amplitude analysis of nonleptonic decays has emerged as an excellent tool for studying charm hadron dynamics. Extensive amplitude analyses have been made for the $D \to K\pi\pi$ final states [1–5]. Measurements of the Cabbibo suppressed $D^+ \to K^+K^-\pi^+$ and Cabbibo favored $D_s^+ \to K^+K^-\pi^+$ decays * to determine the resonant and three-body nonresonant contributions have been reported [6]. In this Letter, we present an amplitude analysis of the $D^+, D_s^+ \to K^+K^-\pi^+$ final states where the contributing decay channels are allowed to coherently interfere. Knowledge of the quantum mechanical decay amplitude from the Dalitz analysis allows one to properly account for interference effects when calculating branching ratios. Here we present a high statistics amplitude analysis of these states using data collected during the 1990-91 run of Fermilab photoproduction experiment E687.

The E687 detector studied the interaction of high energy ($\simeq$ 200 GeV) photons on a beryllium target. The detector is a large aperture, fixed target, multiparticle, magnetic spectrometer with excellent Čerenkov particle identification and vertexing capabilities. Charm secondary vertices were isolated using a 12 plane microstrip system. A more complete description of the detector appears in Reference [7].

## II. CANDIDATE SELECTION

Two complementary approaches were used to reconstruct primary (charm production) and secondary (charm decay) vertices in our sample. These were called the "candidate driven" vertex method and the "stand alone" vertex method [7]. In the former method, candidate final-state tracks were tested to form a common secondary vertex with a confidence level exceeding 1%. A "seed" track which passes through the secondary vertex and was

---

*Throughout this paper, when referencing a particular state we implicitly include its charge conjugate.

directed along the $D$ candidate's momentum vector was used to search for the primary vertex. The vertex finder reconstructed the primary vertex by searching for tracks which formed high confidence level intersections with the seed track. Track parameter errors were propagated through this algorithm. Tracks were added to the primary vertex as long as the confidence level of the resulting vertex exceeded 1%. By way of contrast, the "stand alone" vertex algorithm found vertices without reference to a particular charm candidate track combination by attempting to reconstruct the whole vertex topology of the event. The "stand alone" vertex finder iteratively intersected tracks to search for high quality, isolated vertices. The central values of our measurements were obtained using the "candidate driven" sample but the consistency with the independently analyzed "stand alone" sample was used to estimate the size of the systematic errors.

We begin by describing the selection of the "candidate driven" $D^+, D_s^+ \to K^+K^-\pi^+$ candidates. Two particles were Čerenkov identified as kaons or kaon/proton ambiguous. The pion candidate was required to be Čerenkov inconsistent with the electron, kaon, kaon/proton and proton hypotheses. These tracks formed the candidate secondary vertex. The primary vertex candidate was required to have at least two tracks in addition to the seed track. The secondary vertex was required to be downstream of the primary vertex by at least 8 standard deviations[†] ($\ell > 8\sigma_\ell$). To ensure the secondary vertex was well isolated, leftover tracks not found in the primary vertex were required to be inconsistent with emerging from the secondary vertex and secondary tracks were required not to point to the primary vertex. To remove significant contamination of the $D_s^+ \to K^+K^-\pi^+$ signal due to Čerenkov misidentified background from the decay mode $D^+ \to K^-\pi^+\pi^+$, we employed an "anti-reflection" cut which rejected candidates which, when reconstructed as $K^-\pi^+\pi^+$, were consistent with

---

[†]The variable $\ell$ is the signed 3 dimensional separation between vertices and $\sigma_\ell$ is the error on $\ell$ computed on an event-by-event basis including effects of multiple Coulomb scattering.

the $D^+$ hypothesis .[‡] This cut had no effect in the vicinity of the $D^+ \to K^+K^-\pi^+$ signal peak, but it removed approximately 20% of the true $D_s^+ \to K^+K^-\pi^+$ signal and created an inefficiency which varied by 25 % across the Dalitz plot. The acceptance variation of this cut was primarily correlated with $M^2_{K^-\pi^+}$ and was independent of the parent $D$ momentum. The resulting $K^+K^-\pi^+$ invariant mass distribution is shown in Fig. 1A.

The invariant mass distribution from the sample obtained with the stand alone vertex finder is shown in Fig. 1B. This signal was brought out with cuts similar to the particle identification and anti-reflection requirements imposed on the candidate-driven sample.

In order to gauge the effects of background, we also analyzed a much cleaner sample of $D^+, D_s^+ \to K^+K^-\pi^+$ decays by imposing the additional requirement that the secondary vertex lie in the "air gap" region which was downstream of our beryllium target and upstream of any spectrometer elements. These "air gap" candidates had significantly less non-charm background as their $K^+K^-\pi^+$ mass distribution shown in Fig. 1C demonstrates.

For the sample in Fig. 1A, on which our results are based, the yield of events from a fit to a Gaussian distribution over a linear background is $915 \pm 39$ and $701 \pm 36$ in the $D^+$ and $D_s^+$ peaks, respectively. The fitted masses are $1869.2 \pm 0.4$ and $1968.1 \pm 0.5$ $MeV/c^2$ for the respective peaks, which are consistent with the world average values [8]. Events having $M(K^+K^-\pi^+)$ in the region $\pm 2\sigma$ from a signal peak ($\sigma = 7.9$ $MeV/c^2$ and 8.9 $MeV/c^2$ for the $D^+$ and $D_s^+$, respectively) were selected for the amplitude fits. Events from the mass sidebands [§] were used to parameterize the background in the signal region, as discussed

---

[‡]We also rejected events whose $K^+K^-$ mass exceeds 1.84 $GeV/c^2$ in order to exclude background due to $D^{*+} \to D^0\pi^+ \to (K^+K^-)\pi^+$.

[§]The two mass sidebands which we used for the $D^+$ were $1.805 < M(K^-K^+\pi^+) < 1.837$ $GeV/c^2$ and $1.893 < M(K^-K^+\pi^+) < 1.925$ $GeV/c^2$. The two mass sidebands which we used for the $D_s^+$ were $1.905 < M(K^-K^+\pi^+) < 1.941$ $GeV/c^2$ and $2.004 < M(K^-K^+\pi^+) < 2.040$ $GeV/c^2$. These sidebands were chosen asymmetrically about the signal peaks because the $D^+$ and $D_s^+$ peaks are

below.

## III. FITTING THE DALITZ PLOTS

The Dalitz plots for the $D^+$ and $D_s^+$ signal regions are shown in Figs. 2 and 3, respectively. The bands due to $D \to \phi\pi^+$ and $D \to \overline{K}^*(892)^0 K^+$ decay are evident for both the $D^+$ and $D_s^+$. The depopulation in the center of both the $\phi$ and $\overline{K}^*(892)^0$ bands is due to a node in the angular wave function describing the decay of these vector resonances into their two pseudoscalar daughters.

Following our previous work [5], we performed maximum likelihood fits to the two $K^+K^-\pi^+$ Dalitz plots to measure the fraction of decays into the intermediate modes as well as their relative phases. We allowed for the possibility of contributions from known $(K^-\pi^+)$ and $(K^+K^-)$ resonances [8]. The total decay amplitude was assumed to consist of a sum over the contributing decay modes of functions $B$ which represent intermediate strong resonances and the decay angular wave function appropriate for the given resonance's spin. The fit parameters** are amplitude coefficients $a_i$ and phases $\delta_i$:

$$\mathcal{A}(D) = \sum_i a_i \; e^{i\delta_i} \; B(a \; b \; c \; | r) \qquad (1).$$

Explicitly, $a, b$, and $c$ label the final state particles, $B(a \; b \; c \; | r) = BW(a, b|r) \; \mathcal{S}(a, c)$ where $BW(a, b|r)$ is the Breit-Wigner function

$$BW(a, b|r) = \frac{F_D F_r}{M_r^2 - M_{ab}^2 - i \; \Gamma \; M_r} \qquad (2)$$

and, $\mathcal{S}(a, c) = 1$ for a spin 0 resonance, $\mathcal{S}(a, c) = (-2 \; \vec{c} \cdot \vec{a})$ for a spin 1 resonance, and

---

fairly close in mass.

**We fix the parameters of the $\overline{K}^*(892)^0 K^+$ decay mode to have amplitude coefficient $a_{K^*} = 1$ and phase $\delta_{K^*} = 0$.

$\mathcal{S}(a,c) = 2(|\vec{c}||\vec{a}|)^2(3\cos^2\theta^* - 1)$ for a spin 2 resonance[††] The $\vec{c}$ and $\vec{a}$ are the three momenta of particles $c$ and $a$ measured in the $ab$ rest frame, and $\cos\theta^* = \vec{c}\cdot\vec{a}/|\vec{c}||\vec{a}|$. The momentum-dependent form factors $F_D$ and $F_r$ represent the strong coupling at each decay vertex. For each resonance of mass $M_r$ and spin $j$ we use a width [3] , $\Gamma = \Gamma_0 \left[\frac{p}{p_0}\right]^{2j+1} \frac{M_0}{M_{ab}} \frac{F_r^2(p)}{F_r^2(p_0)}$, where $p$ is the decay momentum in the resonance rest frame and the 0 subscript denotes the rest mass values. [‡‡]

The order of particle labels is important in defining our phases (eg. for vector decays, exchanging $a$ and $b$ results in phase shift of 180 degrees). $B(a\ b\ c|r)$ was computed according to $B(\pi^+K^-K^+|(K^-\pi^+))$ for $(K^-\pi^+)$ resonances and $B(K^+K^-\pi^+|(K^+K^-))$ for $(K^+K^-)$ resonances.

The amplitudes were weighted by a function to correct for geometrical acceptance and reconstruction efficiency. Efficiency variation across the Dalitz plot was less than 30%. Monte Carlo studies confirmed that biases caused by finite mass resolution were negligible.

The shape of the background contribution was parameterized from polynomial fits to the mass sideband Dalitz plots including terms up to $[M^2_{K^-\pi^+}M^2_{K^+K^-}]^3$. The number of background events expected in the signal region was determined from fits to the $K^+K^-\pi^+$

---

[††]We searched for decays through intermediate resonances of spin 3 but found insignificant contributions from those modes.

[‡‡]To retain consistency with our formalism, we employed a modified version of the parameterization described by the WA76 collaboration [9] for the $f_0(980)$ amplitude , which is written $BW(a,b|r) = \frac{F_D F_r}{M_r^2 - M_{ab}^2 - i\,(\Gamma_\pi + \Gamma_K)\,M_r}$, with $\Gamma_\pi = g_\pi \left[\frac{M^2_{K^-K}}{4} - M^2_\pi\right]^{1/2}$ and $\Gamma_K = \frac{g_K}{2}\left[\left(\frac{M^2_{K^+K^-}}{4} - M^2_{K^+}\right)^{1/2} + \left(\frac{M^2_{K^+K^-}}{4} - M^2_{K^0}\right)^{1/2}\right]$. For the coupling constants we use the WA76 values, $g_\pi = 0.28 \pm 0.04$ and $g_K = 0.56 \pm 0.18$. We found that our parameterization of the $f_0(980)$ amplitude imposed approximately 1% systematic uncertainty in the decay fractions of the landmark resonances.

invariant mass distribution consisting of Gaussian signal peaks over linear backgrounds.[§§]

The uncertainties in both the background shape parameters and normalization were included in our statistical error. All background parameters were included as additional fit parameters, but were tied to the results of the sideband fits through the inclusion of a $\chi^2$ contribution to the likelihood constructed using the error matrix from the sideband fits.

We separately fit the $D^+$ and $D_s^+$ samples by forming likelihood functions $\mathcal{L}$ consisting of signal and background probability densities. We minimized the functions $-2\ln\mathcal{L}$ over the signal variables $a_i$ and $\delta_i$. The decay fraction into a given mode was computed by integrating the signal intensity for that mode alone divided by the integrated intensity with all modes present.[***] These fractions do not sum to unity due to the presence of interference between the modes.

The fit quality was evaluated in two ways. In the first method, which was used by Ref. [3], we computed a confidence level using the final value of the likelihood function from the fit and a table of likelihood values derived from repeated Monte Carlo simulations of the experiment assuming as input our final fit result. All fits discussed in this paper returned a confidence level exceeding 34% using this method. In the second method, we assess goodness of fit by calculating a $\chi^2$ which compares the two-dimensional Dalitz plot distribution to the intensity function integrated over bins chosen adaptively such that the predicted number

---

[§§]We were concerned that the anti-reflection cut might significantly distort the mass distribution for charm reflection backgrounds. We confirmed that our fits reliably estimated the fraction of background in the signal region even for the case of charm reflections by using a PYTHIA [12] based photon-gluon fusion Monte Carlo where charm pairs of all species are allowed to decay according to their known decay modes.

[***]This definition, which has become conventional, allows direct comparison of fit results which are independent of the choice of amplitude formalism.

of events in each comparison bin was at least 10 events.[†††] The second method is often the more stringent criterion for goodness-of-fit because it tests the fit's match to the data along both the likelihood gradient and contours of constant likelihood.

Checks of the fitting procedure were made using Monte Carlo techniques and all biases were found to be small compared to the statistical errors. The systematic errors in the decay fractions and phases reflect uncertainties in reconstruction efficiency and background parameterization. For example, because our reconstruction and trigger efficiency is a strong function of the $D$ momentum we compared the fit results from separate fits to the Dalitz plot for candidates both below and above the observed mean $D$ momentum. We also varied the background parameterization, and compared fit results of the full and "air gap" sample. We considered various mass dependent forms for the Breit-Wigner amplitudes [10] and have included any variations in the quoted errors. These effects plus the variation induced by employing the "stand alone" vertexing method are included in the second error bar. Systematic uncertainty due to the statistical errors reported for the $(K^-\pi^+)$ and $(K^+K^-)$ resonance parameters [8] were found to be negligibly small and are not quoted in the tables as separate errors.

## IV. RESULTS FOR THE $D^+ \to K^+K^-\pi^+$ FINAL STATE

As illustrated in the $D^+ \to K^+K^-\pi^+$ Dalitz plot, Fig. 2, the most prominent channels in this decay are $\overline{K}^*(892)^0K^+$, $\phi\pi^+$ and at least one additional slowly varying (in the mass-

[†††]We report both the $\chi^2$ and the number of degrees of freedom in the standard way for a binned distribution. However, we found that the integral of the $\chi^2$ distribution for sets of simulated events is often better matched to a confidence level computed using a degree of freedom which is larger than the number of bins minus the number of fit parameters. We believe that the "miscounting" of the number of degrees of freedom is due to the fact that we minimized the negative log likelihood rather than the $\chi^2$ which was used as the test statistic.

squared variables) resonant or nonresonant contribution. The asymmetry evidenced by the $\phi$ lobes labeled $L_1$ and $L_2$ on the the $M^2_{K^-\pi^+}$ projection, Fig. 4, suggests the presence of a high mass $K^-\pi^+$ resonance. After exploring all known [8] broad resonances in this mass region, we found that the inclusion of a $\overline{K}^*_0(1430)^0 K^+$ contribution can reproduce this lobe asymmetry .[††] The final result is illustrated in Fig. 4 and listed in Table I. Although the mass projections of the fit shown in Fig. 4 are a fairly good match to the mass projection histograms of the data, the fit has an unacceptably large $\chi^2$ for matching the data in adaptively chosen, two dimensional bins (94.2 for 44 degrees of freedom). This suggests that the model, although fitting the data fairly well in a qualitative sense, may be over simplified. For example, there may be contributions from slowly varying, nonresonant amplitudes. We found similar problems in our attempts to fit the $D^+, D^0 \to K\pi\pi$ Dalitz plots [5].

An important application of the present Dalitz amplitude analysis is the extraction of branching ratios both into the inclusive $D^+ \to K^+K^-\pi^+$ final state, as well as into resonant modes. Often [8] for convenience, "branching ratios" are quoted for the decays of charmed particles into particular intermediate state resonant modes (eg. $D^+ \to \phi\pi^+$) which because of the possibility of interference should actually be described by amplitudes rather than partial widths. We quote "branching ratios" into the $D^+$ intermediate two-body resonant states to allow comparison of our results with other groups in Table III. The amplitude fits described here automatically take into account the small but non-negligible effects of interference as well as providing a detailed intensity model for correcting the inclusive yield to account for non-uniformities in the acceptance across the Dalitz plot.[‡‡]

---

[††]The inclusion of additional resonances or nonresonant contribution does little to improve the $\chi^2$ or appearance of the fit projections.

[‡‡]These efficiency variations can come from both apparatus effects as well as the need to impose a kinematic cut to eliminate reflections such as the $D^+ \to K^-\pi^+\pi^+$ reflection background to

We have resisted the temptation to quote branching ratios for any of the $D^+$ decays mentioned in Table I other than the landmark final states $\overline{K}^*(892)^0K^+$ and $\phi\pi^+$ or to set an upper limit on nonresonant (phase space) $K^+K^-\pi^+$ decays. Although we have presented evidence for the presence of each of the broad resonances included in our fits, we lack sufficient statistics to exclude alternative fits where the set of resonance contributions is expanded. Because of interference effects, these broad resonance contributions can fluctuate significantly in expanded fits while the the landmark $\overline{K}^*(892)^0K^+$ and $\phi\pi^+$ contributions remain stable within quoted errors.

We extract the relative branching ratio for $D^+ \to \phi\pi^+$ by using the following formula:

$$\frac{\Gamma(D^+ \to \phi\pi^+)}{\Gamma(D^+ \to K^-\pi^+\pi^+)} = \frac{\Gamma(D^+ \to K^+K^-\pi^+)}{\Gamma(D^+ \to K^-\pi^+\pi^+)} \times \frac{f(D^+ \to \phi\pi^+)}{B(\phi \to K^+K^-)} \tag{3}$$

The term $\frac{\Gamma(D^+ \to K^+K^-\pi^+)}{\Gamma(D^+ \to K^-\pi^+\pi^+)}$ is the ratio of our efficiency corrected yields for $D^+ \to K^+K^-\pi^+$ and $D^+ \to K^-\pi^+\pi^+$ [§§] and has a value of $0.0976 \pm 0.0042 \pm 0.0046$. The factor $f(D^+ \to \phi\pi^+)$ is the decay fraction from Table I and $B(\phi \to K^+K^-)$ is the absolute branching fraction [8] for the $\phi \to K^+K^-$. The $D^+ \to \overline{K}^*(892)^0K^+$ branching ratio is similarly calculated. We compare our measured branching ratios to other recent measurements in Table III.

## V. RESULTS FOR THE $D_S^+ \to K^+K^-\pi^+$ FINAL STATE

As Fig. 3 shows, the $D_s^+ \to K^+K^-\pi^+$ Dalitz plot is very strongly dominated by the $\overline{K}^*(892)^0K^+$ and $\phi\pi^+$ decays. The Dalitz plot for the relatively background free "air gap" sample, shown in Fig. 3C, shows an accumulation of events in the nodal region of the $\phi$ band. After studying contributions from known $(K^+K^-)$ and $(K^-\pi^+)$ resonances, we found that the decay $D_s^+ \to f_0(980)\pi^+$ is the most likely source responsible for this accumulation.

---

$D_s^+ \to K^+K^-\pi^+$.

[§§]Our $K^-\pi^+\pi^+$ sample was reconstructed using the candidate driven vertex algorithm and was subjected to cuts similar to the $K^+K^-\pi^+$ sample.

The intensity for simulated $D_s^+ \to f_0(980)\pi^+$ decays tends to cluster at the low $M^2_{KK}$ masses and populate the $\phi$ nodal region. The $f_0(980)$ decays via both $\pi^+\pi^-$ and $K^+K^-$. Because a large fraction of $D_s^+ \to \pi^+\pi^+\pi^-$ decays are known [11] to proceed via $D_s^+ \to f_0(980)\pi^+$, one expects to observe contributions from $D_s^+ \to f_0(980)\pi^+$ to the $K^+K^-\pi^+$ Dalitz plot as well. Upon fitting the full sample to a coherent sum of $\overline{K}^*(892)^0K^+$, $\phi\pi^+$ and $f_0(980)\pi^+$ amplitudes we obtained the projections shown in Fig. 5A. This fit fails to reproduce much of the detailed structure observed in the mass-squared projections, especially around the $\overline{K}^*(892)^0$ peak in the $M^2_{K^-\pi^+}$ projection (Region 1 in Fig. 5A) and the region between the $\overline{K}^*(892)^0$ peak and the $\phi$ lobes on the $M^2_{K^-\pi^+}$ projection (Region 2). In particular, the $K^-\pi^+$ invariant mass near the $\overline{K}^*(892)^0$ peak is shifted significantly lower than the world average value [8] and the fitted $\overline{K}^*(892)^0$ mass of the two $\overline{K}^*(892)^0$ lobes differ.[§§] These observations suggest the presence of additional amplitudes which interfere with the $\overline{K}^*(892)^0$. After studying contributions from established $(K^+K^-)$ and $(K^-\pi^+)$ resonances, we found the inclusion of contributions from $f_J(1710)\pi^+$ and $\overline{K}_0^*(1430)^0K^+$ significantly improved the agreement between the fit and data in Regions 1 and 2, as shown in Fig. 5B.[§] The results of the $D_s^+$ fit are summarized in Table II.

## VI. CONCLUSIONS

In summary, our fits to the $D^+, D_s^+ \to K^+K^-\pi^+$ Dalitz distributions, assuming a model with Breit-Wigner amplitudes for the two-body resonant modes, qualitatively reproduce many features of our data, without the need for a nonresonant component, although statistically significant discrepancies are observed in our fits. The contributions to the $D^+$ decay amplitude were $\overline{K}^*(892)^0K^+$, $\phi\pi^+$, and $\overline{K}_0^*(1430)^0K^+$ whereas the $\overline{K}^*(892)^0K^+$, $\phi\pi^+$,

---

[§§]The fitted masses of the low and high $M^2_{K^+K^-}$ $\overline{K}^*(892)^0$ lobes were $888 \pm 5\ MeV/c^2$ and $876 \pm 5\ MeV/c^2$, respectively, which are both below the world average [8] value $896.10 \pm 0.28\ MeV/c^2$.

[§]In this fit the $f_J(1710)$ is assumed to be a scalar particle.

$f_0(980)\pi^+$, $f_J(1710)\pi^+$ and $\overline{K}_0^*(1430)^0K^+$ were the contributions used in our fits to the $D_s^+$ amplitude. We use our fitted amplitudes to extract improved values for the branching ratios for inclusive $D^+ \to K^+K^-\pi^+$ as well as the exclusive $\phi\pi^+$ and $\overline{K}^*(892)^0K^+$ channels.

We wish to acknowledge the assistance of the staffs of the Fermi National Accelerator Laboratory, the INFN of Italy, and the physics departments of the collaborating institutions. We also wish to acknowledge useful discussions with Dr. Phil Ratcliffe of the Milan University. This research was supported in part by the National Science Foundation, the U.S. Department of Energy, the Italian Istituto Nazionale di Fisica Nucleare and Ministero dell'Università e della Ricerca Scientifica e Tecnologica, and the Korean Science and Engineering Foundation. Dr. Vincenzo Arena wishes to acknowledge the support of the Fondazione Angelo Della Riccia.

# REFERENCES

[a] Present address: Fermilab, Batavia, IL 60510, USA.

[b] Present address: University of Maryland, College Park, MD 20742, USA.

[c] Present address: University of Colorado, Boulder, CO 80309, USA.

[d] Present address: University of New York, Stony Brook, NY 11794, USA.

[e] Present address: Yale University, New Haven, CN 06511, USA.

[f] Present address: Pohang Accelerator Laboratory, Pohang, Korea.

[g] Present address: Lawrence Berkeley Laboratory, University of California, Berkeley, CA 94720, USA.

[h] Present address: Enrico Fermi Institute, University of Chicago, Chicago, IL 60637, USA

[1] MARK III Collab., J. Adler *et al.*, Phys. Lett. B 196 (1987) 107.

[2] E687 Collab., P.L. Frabetti *et al.*, Phys. Lett. B 286 (1992) 195.

[3] ARGUS Collab., H. Albrecht *et al.*, Phys. Lett. B 308 (1993) 435.

[4] E691 Collab., J.C. Anjos *et al.*, Phys. Rev. D 48 (1993) 56.

[5] E687 Collab., P.L. Frabetti *et al.*, Phys. Lett. B 331 (1994) 217.

[6] E691 Collab., J.C. Anjos *et al.*, Phys. Rev. Lett. 60 (1988) 897.

[7] E687 Collab., P.L. Frabetti *et al.*, Nucl. Instrum. Methods. A 320 (1992) 519;
E687 Collab., P.L. Frabetti *et al.*, Nucl. Instrum. Methods. A 329 (1993) 62.

[8] Particle Data Group, L. Montanet *et al.*, Phys. Rev. D 50 (1994) 1173.

[9] WA76 Collab., T.A. Armstrong *et al.*, Z. Phys. C 51 (1991) 351.

[10] MARK III Collab., D. Coffman *et al.*, Phys. Rev. D 45 (1992) 2196.

[11] E691 Collab., J.C. Anjos *et al.*, Phys. Rev. Lett. 62 (1989) 125.

[12] T.Sjostrand, Computer Phys. Comm. 39 (1986) 347;
T.Sjostrand, H.-U.Bengtsson, Computer Phys. Comm. 43 (1987) 367;
H.-U.Bengtsson, T.Sjostrand, Computer Phys. Comm. 46 (1987) 43.

[13] MARK III Collab., R.M.Baltrusaitis *et al.*, Phys. Rev. Lett. 55 (1985) 150.

[14] WA82 Collab., M. Adamovich *et al.*, Phys. Lett. B 305 (1993) 177.

[15] CLEO Collab., M. Daoudi *et al.*, Phys. Rev. D 45 (1992) 3965.

[16] NA14 Collab., M.P. Alvarez *et al.*, Phys. Lett. B 246 (1990) 261.

## TABLES

TABLE I. Dalitz plot fit results for the $D^+ \to K^+K^-\pi^+$ final state. In Tables I-II, the first error is statistical and the second is systematic.

| Decay mode | Decay fraction | Phase(degrees) | |
|---|---|---|---|
| $\overline{K}^*(892)^0K^+$ | $0.301 \pm 0.020 \pm 0.025$ | 0 (fixed) | |
| $\phi\pi^+$ | $0.292 \pm 0.031 \pm 0.030$ | $-159 \pm 8 \pm 11$ | |
| $\overline{K}_0^*(1430)^0K^+$ | $0.370 \pm 0.035 \pm 0.018$ | $70 \pm 7 \pm 4$ | |
| Goodness of fit | $-2\ln\mathcal{L} = -723$ | $\mathcal{L}$ conf. level = 34.2% | $\chi^2 = 92.2$ (44 dof) |

TABLE II. Dalitz plot fit results for the $D_s^+ \to K^+K^-\pi^+$ final state.

| Decay mode | Decay fraction | Phase (degrees) | |
|---|---|---|---|
| $\overline{K}^*(892)^0K^+$ | $0.478 \pm 0.046 \pm 0.040$ | 0 (fixed) | |
| $\phi\pi^+$ | $0.396 \pm 0.033 \pm 0.047$ | $178 \pm 20 \pm 24$ | |
| $f_0(980)\pi^+$ | $0.110 \pm 0.035 \pm 0.026$ | $159 \pm 22 \pm 16$ | |
| $f_J(1710)\pi^+$ | $0.034 \pm 0.023 \pm 0.035$ | $110 \pm 20 \pm 17$ | |
| $\overline{K}_0^*(1430)^0K^+$ | $0.093 \pm 0.032 \pm 0.032$ | $152 \pm 40 \pm 39$ | |
| Goodness of fit | $-2\ln\mathcal{L} = -1075$ | $\mathcal{L}$ conf. level = 80.2% | $\chi^2 = 50.2$ (33 dof) |

TABLE III. Ratios of Partial Widths

| Exp. | $\frac{\Gamma(D^+\to\overline{K}^*(892)^0K^+)}{\Gamma(D^+\to K^-\pi^+\pi^+)}$ | $\frac{\Gamma(D^+\to\phi\pi^+)}{\Gamma(D^+\to K^-\pi^+\pi^+)}$ |
|---|---|---|
| E687 (this work) | $0.044 \pm 0.003 \pm 0.004$ | $0.058 \pm 0.006 \pm 0.006$ |
| CLEO [15] | | $0.077 \pm 0.011 \pm 0.005$ |
| NA14 [16] | | $0.098 \pm 0.032 \pm 0.014$ |
| WA82 [14] | | $0.062 \pm 0.017 \pm 0.006$ |
| E691 [6] | $0.058 \pm 0.009 \pm 0.006$ | $0.071 \pm 0.008 \pm 0.007$ |
| MARK III [13] | $0.048 \pm 0.021 \pm 0.011$ | $0.084 \pm 0.021 \pm 0.011$ |

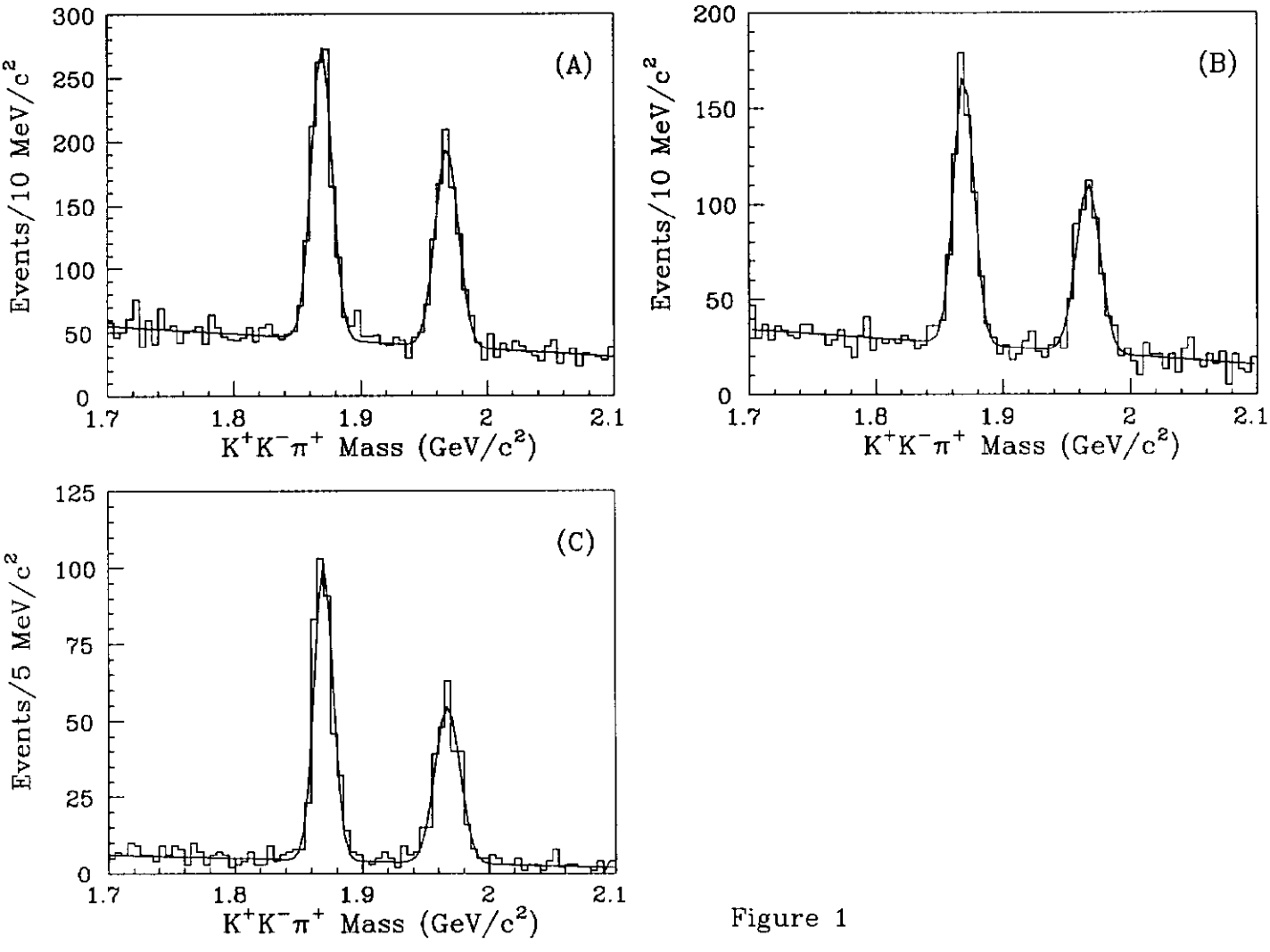


Figure 1

FIG. 1. Invariant mass distribution for $D^+, D_s^+ \to K^+K^-\pi^+$ candidates: A) the full data sample from the candidate driven vertex finder; B) the full sample from the stand alone vertex finder; C) the "air gap" sample from the candidate driven vertex finder. The curves show the fits used to estimate the signal yields and background fractions.

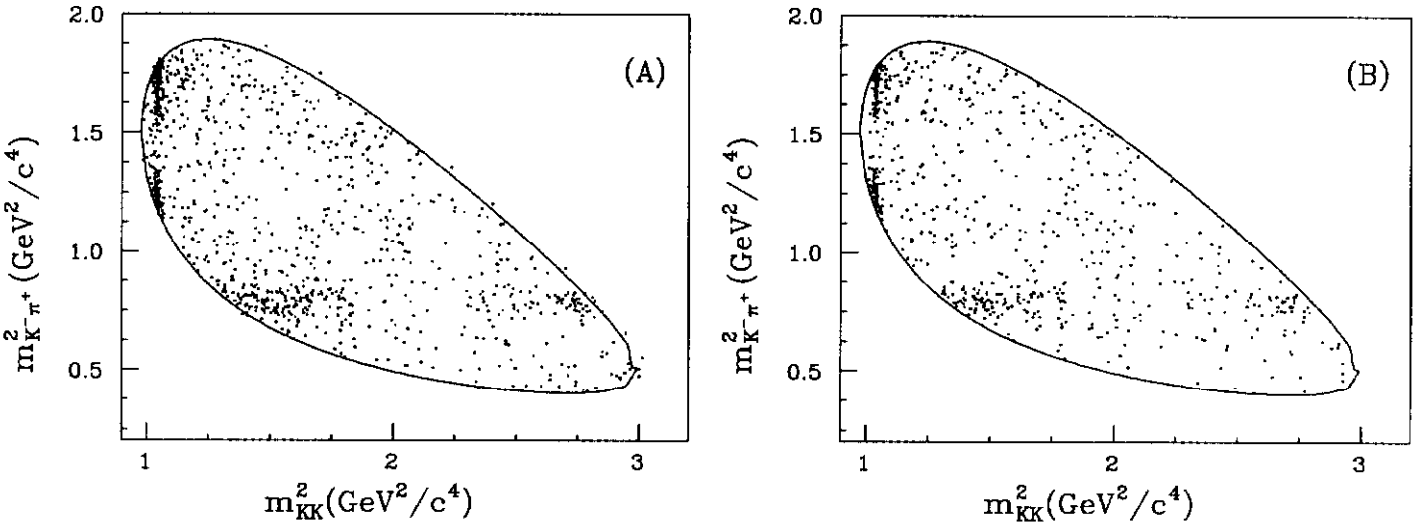


Figure 2

FIG. 2. Dalitz plots for the decay $D^+ \to K^+K^-\pi^+$: A) the full data sample from the candidate driven vertex finder; B) the full sample from the stand alone vertex finder.

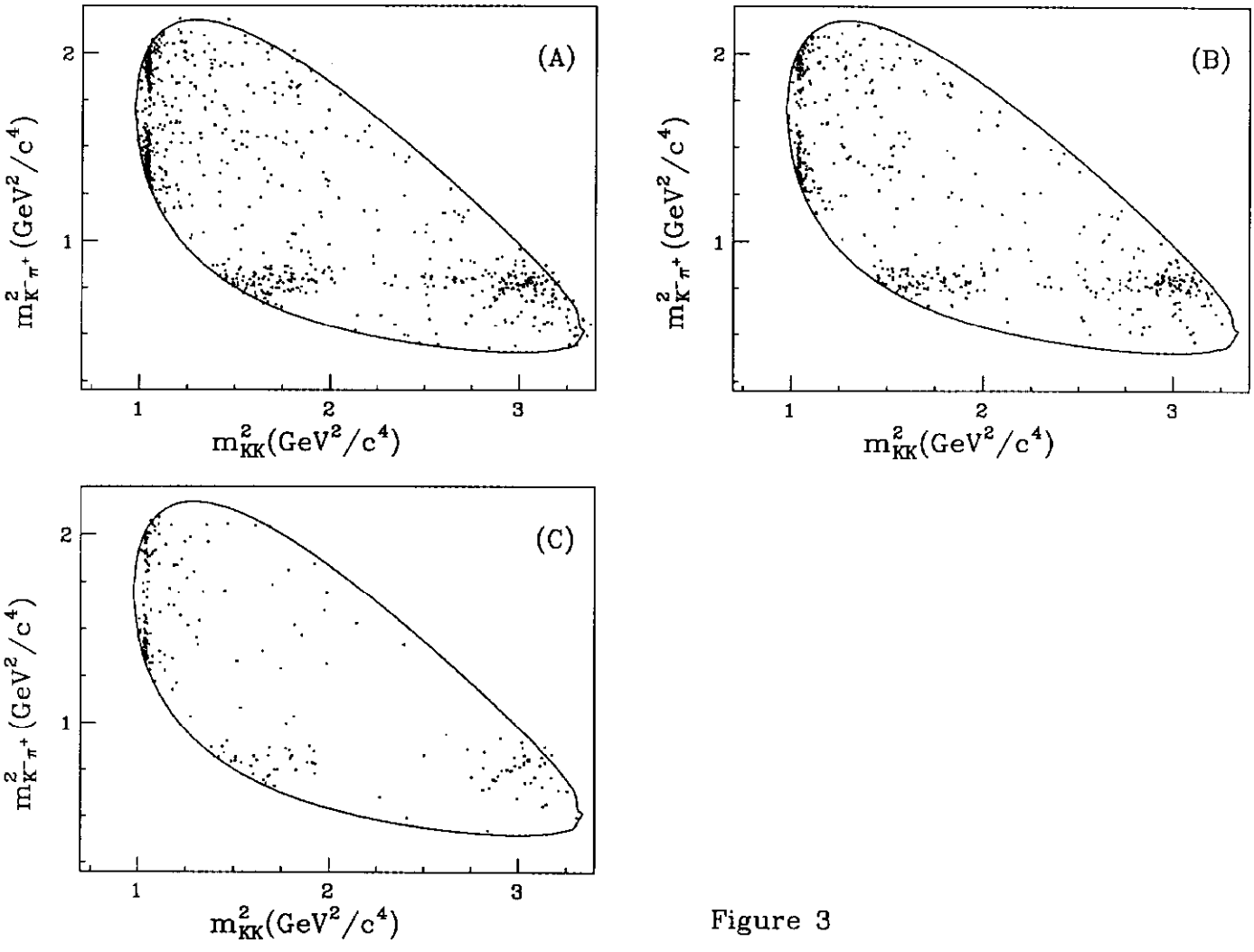


Figure 3

FIG. 3. Dalitz plots for the decay $D_s^+ \to K^+K^-\pi^+$: A) the full data sample from the candidate driven vertex finder; B) the full sample from the stand alone vertex finder; C) the "air gap" sample from the candidate driven vertex finder.

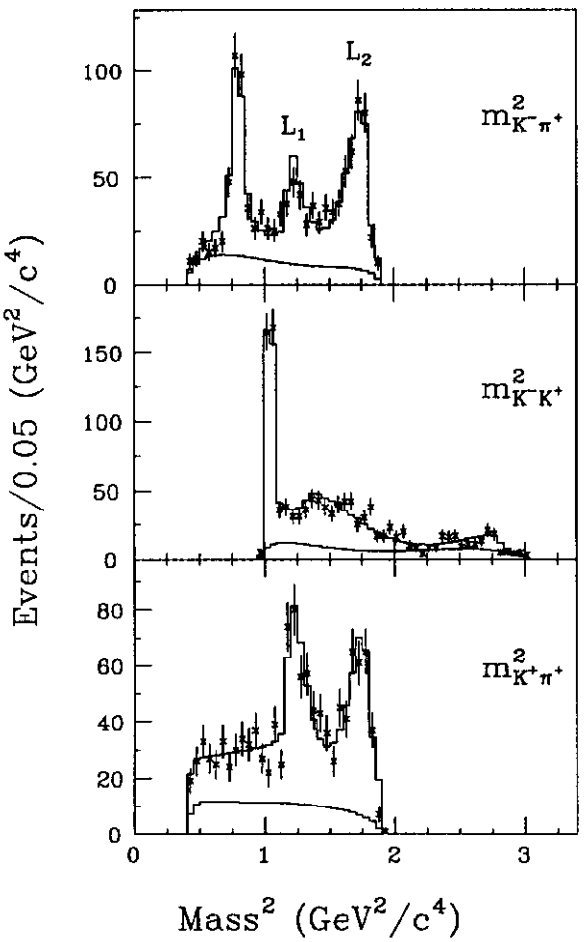


Figure 4

FIG. 4. Mass-squared projections for the decay $D^+ \to K^+K^-\pi^+$. In Figs. 4 and 5, the data are represented by points, and in each mass-squared projection the upper histogram describes the predicted signal plus background contribution as determined by the fit, and the lower histogram represents the background contribution. These results are from fits to the full data sample obtained with the candidate driven vertex finder.

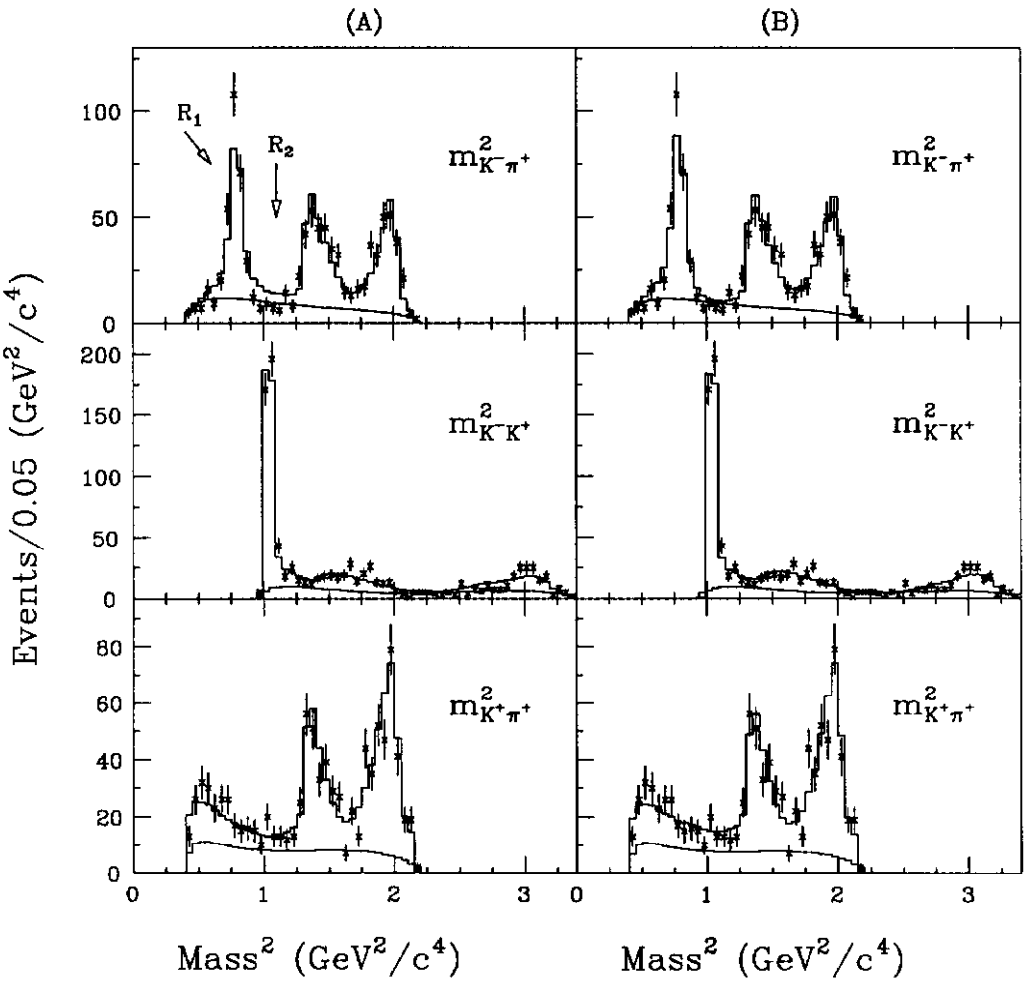


Figure 5

FIG. 5. Mass-squared projections for the decay $D_s^+ \to K^+K^-\pi^+$. The projections in A) were calculated with a superposition of $\overline{K}^*(892)^0K^+$, $\phi\pi^+$ and $f_0(980)\pi^+$ amplitudes while the B) solution includes contributions from the $f_J(1710)$ and $\overline{K}_0^*(1430)^0K^+$ amplitudes.